Eidgenössische Technische Hochschule Zürich
Swiss Federal Institute of Technology Zurich

Short Term Stability Optimization of a Frequency Doubling Cavity

Semester Thesis

Nicola Meggiato
nmeggiato@student.ethz.ch

Trapped Ion Quantum Information Group
Department of Physics
ETH Zürich

Supervisors:
David Holzapfel,
Dr. Daniel Kienzler,
Prof. Dr. Jonathan Home

June 2022

Contents

1 Introduction

UV lasers find application in many research and technological areas such as micromachining and medicine. Fundamental is their role in the quantum computing branch of trapped ion quantum information. For example, when dealing with Beryllium ions ($^9Be^+$), their electric dipole transition energy separating the states $S_{1/2}$ and $P_{3/2}$, corresponds to $\lambda = 313.133$ nm which falls in the UV spectrum.
Furthermore, in order to effectively cool and detect the ions, one needs highly stable beam with a well defined power. UV radiation can be created in free electron or Argon lasers. This requires relatively complex setups which can be expensive and inefficient. However, it is possible to efficiently obtain UV lasers from more accessible laser frequencies. This requires exploiting a non-linear process called Second Harmonic Generation (SHG) [1]. This physical phenomenon happens in non-linear crystals, objects characterized by a non-negligible second order polarizability $\chi^{(2)}$. This basically implies that the emitted radiation of dipoles in the crystal under the excitation of a laser beam at frequency ω_{ic} (pump beam) is in some part oscillating at $\omega_0 = 2\omega_{ic}$ [1]. The second order polarizability is typically much lower than the first, so high power pump beams are needed. Due to the high power required, the process typically happens in frequency doubling cavities [2].
In the Molecules subgroup [3] of the Trapped Ion Quantum Information group (TIQI) at ETH Zürich, three doubling cavities are used, two of which will be discussed in the report. The first serves for detection and cooling of the ion. The needed beam for that is obtained starting from a 626.266 nm laser beam generated in room B20, which is transmitted by a optical fiber to B104, where it is coupled to the "Resonance" cavity. Using acousto-optic modulators (AOMs), the resulting UV light (with a power of $\sim 5 - 10$ mW) can be further shifted in frequency depending on the respective application. Similarly, a second 626 nm laser beam is taken from the Penning setup and subsequently converted to 313 nm beam by the "Raman" cavity. Within this work, also two similar doubling cavities in the Penning setup will be evaluated, labelled "Repump" and "Detection".

All the doubling cavities in the lab follow the scheme reported in Fig. 1a. The 626 nm pump laser impinges on a semi-transparent mirror (1) and is coupled into the cavity. As demonstrated in the scheme of Fig. 1a, the cavity consists of four mirrors, that guide the light on a characteristic Bow-tie path. The nonlinear crystal, BBO (barium borate) in this case, is placed in the light path. Optical cavities are resonators where only laser beams with a resonant frequency can form standing waves, while off-resonant beams would not be sustained due to destructive interference. Both the laser frequency and the cavity length are subject to environmental disturbances, so the process of keeping the cavity length at a certain value such that the pump laser results resonant for the cavity, called "cavity locking", is needed.
In Molecules' setup, Pound-Drever-Hall-locking (PDH-locking) [4] stabilization scheme is implemented for this purpose. A picture of one of the "Resonance" doubing cavity in the molecules setup is shown in Fig. 1b.

Given the key role that UV beams have in the experiments, a certain level of stability and robustness to environmental noise is required for frequency doubling cavities.
Due to observations of instability to, for instance, acoustic noise, a deeper understanding of what could cause it, became relevant. Piezo-chips are known to possess resonant frequencies at which the driving signal has much higher piezoelectric response [5]. Given their application in the setup, the investigation of how these reflect in the doubling cavities' instability followed naturally. In this project, the main goal was to characterize the doubling cavities' electrical and acoustic noise response to be able to compare the results and gain better knowledge of our systems. Furthermore, attempts of finding better performance mount - piezo-chip - mirror (MPM) systems used in the cavities (piezo-actuated mirrors) were made.

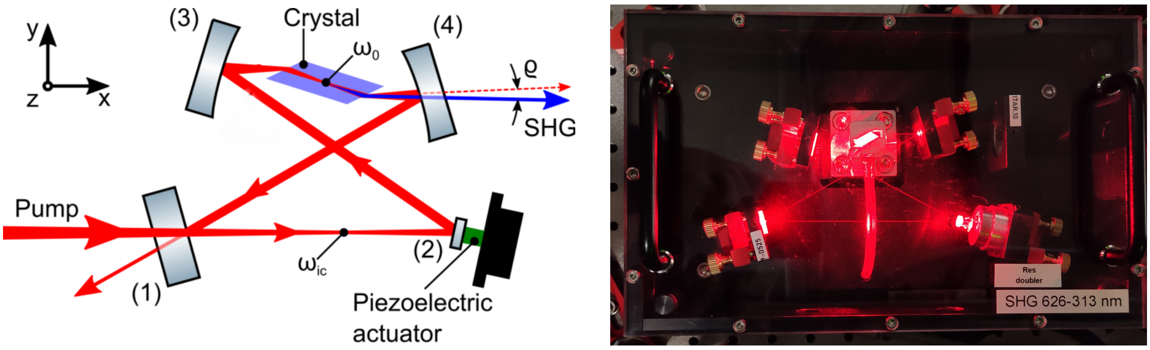

(a) (b)

Figure 1: (a): Schematic of a Bow-tie frequency doubling cavity. The pump laser at frequency ω_{ic} is locked to the cavity and forms a standing wave. The second harmonic generation in the crystal leads the secondary frequency-doubled beam (at ω_0) to be transmitted with a relative angle ρ with respect to the pump beam. (b): Image of the ”Resonance” frequency doubling cavity in the Molecules’ setup. The standing wave becomes visible in the doubling cavity as long as the latter is properly locked.

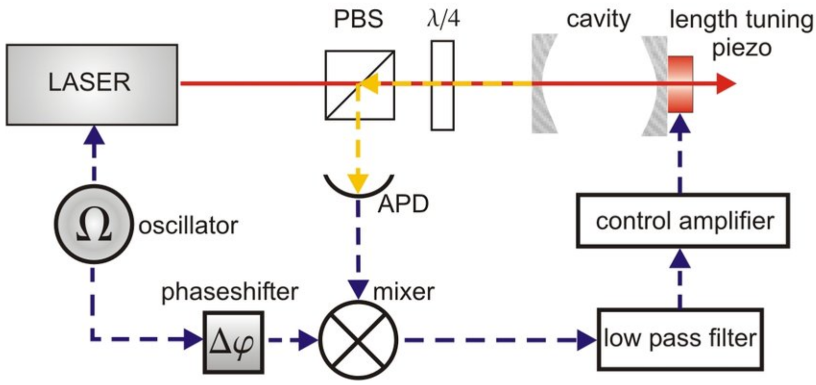

Figure 2: PDH locking scheme, adapted from [7].
The laser is modulated by an rf signal. The laser beam interacts with the cavity and is partially reflected to a photodiode. The so obtained signal is mixed with the same rf signal. In this way the error signal is transmitted to the control amplifier which drives the piezoelectric element.

2 Characterization of doubling cavities

2.1 Control system and PDH locking

As already mentioned, to be able to generate a UV beam via a doubling cavity even if noise leads to small shifts in the optical path length inside the cavity, the latter is kept locked with a PDH locking scheme. A sketch of it is shown in 2. Details of the working principle of this technique can be found in [6], where the opposite yet analogous approach of locking a tunable laser frequency to the cavity is described.

The pump laser is transmitted into the cavity, which is kept at the right optical length by a piezoelectric actuated mirror. The piezoelectric element is driven by a control amplifier with the goal of adjusting its length. For this purpose, the amplifier receives a so called error signal e as input. The error signal generation is not trivial, and requires the use an rf signal from a local oscillator. This signal has two purposes. The first is to modulate the laser (more details later), while the second is to mix it with the photo-generated signal coming a partial reflection of the laser after having interacted with the cavity.

The simplified sketch of the actual implementation of this model in the molecules setup is illustrated in Fig. 3. Here, the 626 nm laser beam is first shined into an Electro-Optical Modulator (EOM) which is generating the sidebands [8], as the PDH scheme requires. Then, after getting partially reflected to a photodiode to obtain signal p, it enters the cavity. The signal is then mixed via KILL (Keitch Integrated Laser Lock) [9] with a known rf signal, which is the same driving the EOM. All this results in the output signal y, which is eventually subtracted from the reference one r. The obtained error signal e is the input signal for the controller. The controller is implemented by EVIL (Electronically Variable Interactive Lock-box), a device that also functions as amplifier for the signal, to properly drive the piezo-chip.

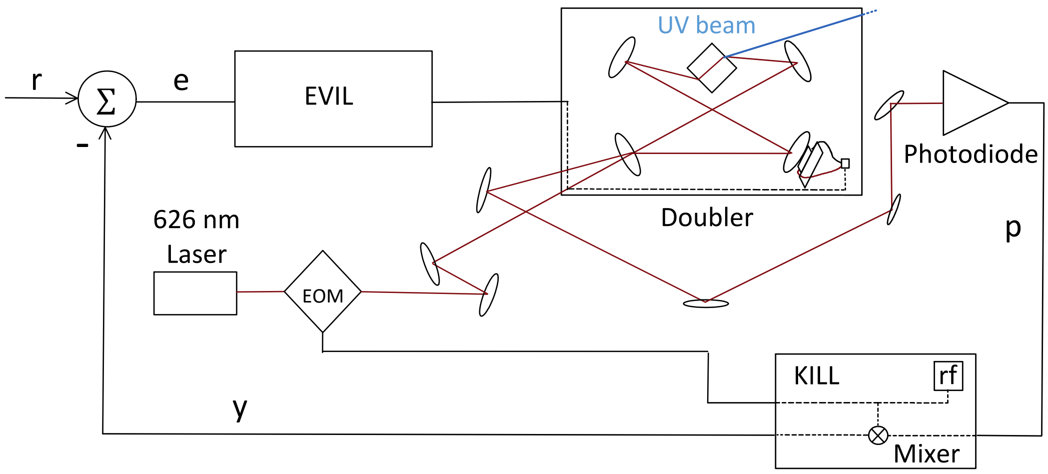

Figure 3: Sketch of the PDH scheme implemented in the Molecules' setup. The cavity follows a bow-tie configuration and together with KILL forms the plant of the system. KILL generates an rf signal and mixes it with p to obtain y. The latter gets subtracted from the reference signal r to create the error signal e. EVIL implements a PID controller and also works as amplifier.

This simple schematic gives us the opportunity to briefly recap some basic control systems theory that will be helpful in the following. As a reference, one could look at [10]. The goal of a controller is to make the target system follow a certain reference signal r with a desired transfer function $T^*(s)$, s being the Laplace frequency.
Various parts in the setup have specific name and roles:

- The system to be controlled is often referred to as "plant" and is modeled by $G(s)$. In our case the plant consists in all the components except for EVIL, which together can be seen as a black-box with input coming from EVIL and output $= y$.
- EVIL implements a PID controller, which will have its own Laplace transfer function from input to output that we label K(s). The general form of a PID controller's transfer function is
$$K(s) = K_p + \frac{K_i}{s} + K_d s \tag{1}$$
which corresponds to a response to an error e(t) in time domain:
$$u(t) = K_p\, e(t) + K_i \int_0^t e(\tau)\, d\tau + K_d \frac{\mathrm{d}e(t)}{\mathrm{d}t} \tag{2}$$
where K_p, K_i, K_d are constants.
- In the experiments the DEVIL GUI allows to choose the value of r, corresponding to set a DC offset to the signal driving the piezo.
- We define $L(s) := K(s)\, G(s)$ to be the open loop transfer function of the system.It translates the input in output when the closed loop is removed.

- We further define the sensitivity and the complementary sensitivity functions, respectively as:

$$\begin{aligned} S(s) &= \frac{1}{1+L(s)} \\ T(s) &= \frac{L(s)}{1+L(s)} \end{aligned} \tag{3}$$

  The two being linked by the following constraint:

$$S(s) + T(s) = 1. \tag{4}$$

The physical meaning of the equations 3 can be deducted by looking at the general scheme for a feedback-controlled system which is shown in Fig. 4.

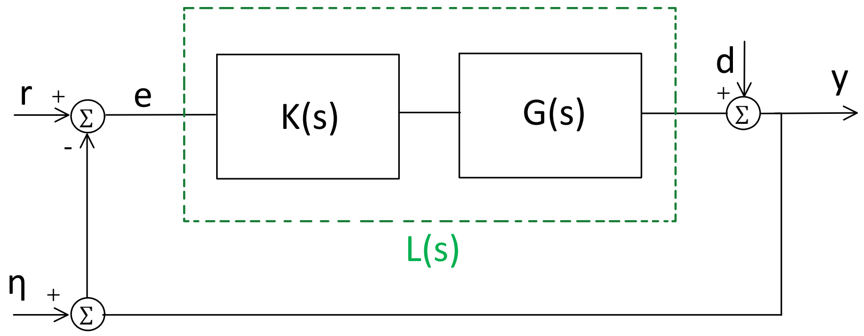

Figure 4: General schematic of a controlled system. The plant is represented by $G(s)$, the controller by $K(s)$. The noise can enter the system at different stages of the loop, the most common of which are before the output (plant noise d) and in the feedback loop η.

From simple calculations one could easily obtain the relation between the output y, the input r, and the two possible sources of noise: entering before the output (plant noise), d, or in the feedback loop, η:

$$\begin{aligned} y &= \frac{L(s)}{1+L(s)}\, r + \frac{1}{1+L(s)}\, d - \frac{L(s)}{1+L(s)}\, \eta \\ &= T(s)\, r + S(s)\, d - T(s)\, \eta. \end{aligned} \tag{5}$$

- T(s) maps the refence signal r and the feedback loop noise η (up to a minus sign) to the output y.
- S(s) represents the transfer function from the noise d to output y.

The desired transfer function from reference to output $T^*(s)$ should be designed to have unitary amplitude and the highest possible servo bandwidth, i.e. the frequency at which the amplitude is reduced by a factor $\frac{1}{\sqrt{2}}$ with respect to the DC.
Typically, we aim to track mostly low frequencies signals r. The plant noise d is mostly due to electronics and has therefore spectral density $S_{xx}(f) \propto 1/f$. The feedback loop noise η is picked up from the environment and therefore is shifted to high frequencies. Furthermore, $S(s)$ and $T(s)$ are constrained by equation 4, so the optimal behaviour of the two is represented in fig. 5.
These requirements follow from the goal of the locking system: to reliably lock the cavity to the laser even in presence of disturbances at different frequencies.

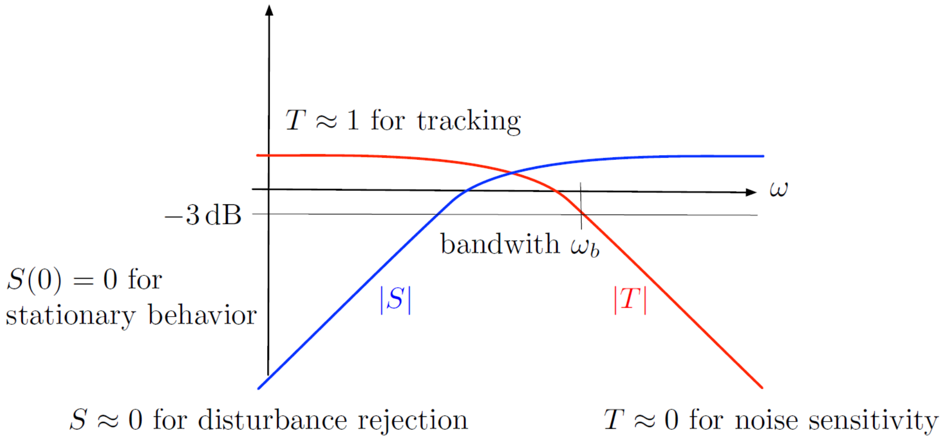

Figure 5: Desirable closed-loop shapes for S (blue) and T (red). The bandwidth is defined as the frequency at which $T(s)$ intercepts the -3 dB horizontal line, meaning that the amplitude response is reduced by $1/\sqrt{2}$[11].

2.2 Electrical noise characterization

The first type of measurement we decided to perform to characterize the doubling cavities' noise response is the electrical one. The final goal was to investigate what are the electrical resonance frequencies of the system by injecting an additional small amplitude probe signal in the loop. This was done to simulate electric disturbances that can interfere in the control system. From now on, we will therefore refer to the probe signal as "noise" η.
At this scope, we set up a measurement scheme as in Fig. 6. This involves the already presented PDH setup and the Analog Discovery Kit 2 (ADK), which is a multi-function instrument that allows users to measure, visualize, generate, record, and control mixed-signal circuits of many kinds [12]. This instrument can be controlled directly via an intuitive GUI (called "Waveforms") using a PC. ADK has two input ports, labeled Ch1 and Ch2 and two output ports, W1 and W2. Thus, the maximum number of channels we could observe is two. In our experiment, we used the network analyzer feature to inject electrical noise sweeping various frequencies ranges and record it with Ch1. At the same time we measured how this affects two specific signals in the loop: e' and y, detected via Ch2. One caveat about the schematic presented in Fig. 6 is that η enters the loop with a negative sign. This is because the summation node at the bottom represents New Focus LB1005 Servo Controller, which allows for adding up two signals with the constraint of them having different sign [13]. The noise is generated by ADK and gets mixed right after the KILL stage, thus directly affecting the error signal that enters EVIL [1]. One should note that this is **not** the only stage of the loop where in principle the noise can get in, as previously illustrated in Fig. 4, but it can be shown that for any choice of the stage in which noise gets into the system, there always are two measurable signals (alternative to e' and y in our scenario) leading to the characterization of the same function S(s) and T(s) of which we are interested.

It follows the simple derivation for the chosen signals:

$$\begin{aligned} -\big(e'L(s) - \eta\big) = e' \qquad &\Longrightarrow \qquad \frac{e'}{\eta} = \frac{1}{1+L(s)} = S(s) \\ -\big(y - \eta\big)L(s) = y \qquad &\Longrightarrow \qquad \frac{y}{\eta} = \frac{L(s)}{1+L(s)} = T(s) \end{aligned} \tag{6}$$

[1] Actually, the subraction of r and $y-\eta$ is performed by EVIL internally. The summation node was sketched outside for clarity.

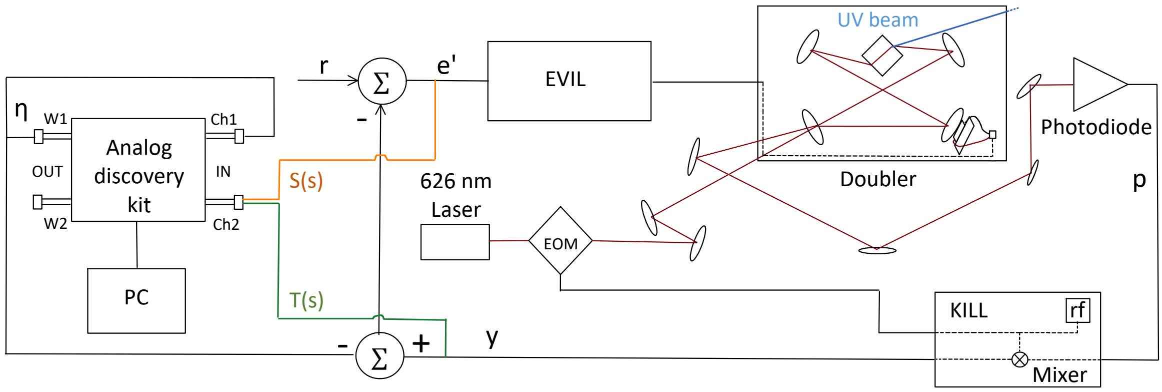

Figure 6: Scheme of the setup for electrical noise characterization. $S(s)$ and $T(s)$ are the transfer function between the injected noise η and, respectively, the measured signals e' and y.

2.2.1 Experimental results

The characterization was performed on both the Molecules' doubling cavities (Raman, Resonance) and one of the Penning's (Repump).

From the measurement procedure detailed in the section above, we were able to compare the different cavities and identify critical electrical resonances in them. As a first observation, we see that the slopes are qualitatively following the ideal behaviour reported in Fig. 5. To discuss the results, the amplitude response for $S(s)$ and $T(s)$ for the Resonance cavity in Fig. 7 are shown. Interested readers find data relative to the other doubling cavities and their phase responses in the appendix A.

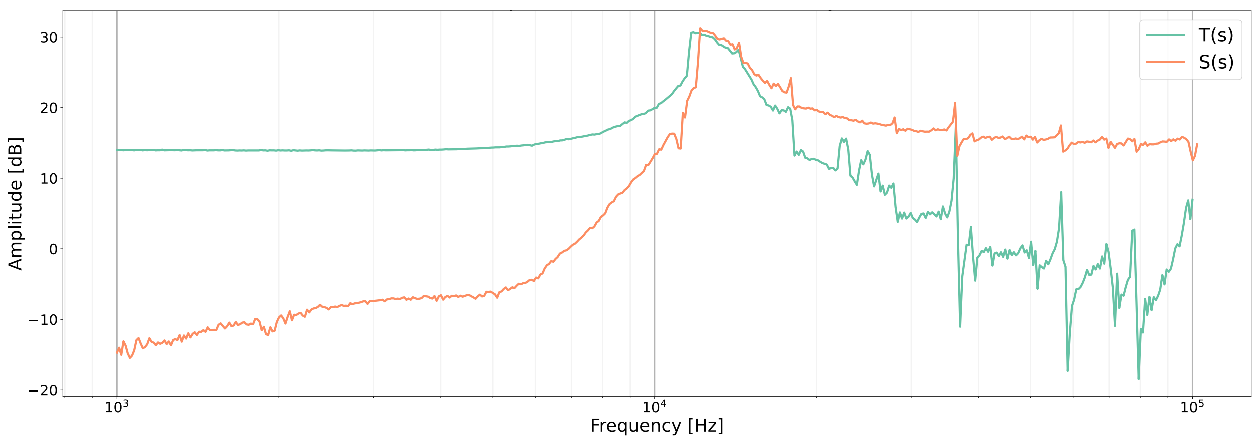

Figure 7: $T(s)$ and $S(s)$ amplitude response for Resonance Cavity. The most relevant resonances are visible in both the transfer functions, but those in $T(s)$ are more pronounced.

The increase in amplitude response around $f = 12$ kHz is the so called "servo bump" and is due to the closed loop configuration.
As a general remark, that applies to all the cavities, one can observe that resonances in $S(s)$ are smaller, therefore leading to good disturbance (d in Fig.4) rejection. Nevertheless we are more interested in the behaviour of $T(s)$, since the noise directly affecting the piezo enters the system as η.

Another high level observation can be done looking at figures 8 and 9. In particular we can observe the better performances of the Raman cavity with respect to the Repump cavity for two reasons. First, the Raman cavity's servo-bump is centered at around 12 kHz, while the Repump cavity's one sits roughly at 8.5 kHz, therefore the second's bandwidth results lower. Secondly, the Raman cavity shows narrower and smaller resonances at high frequencies with respect to the Repump's, particularly visible in the phase response in Fig. 9. On the other hand, the Repump cavity manifests broader resonances, leading to have a greater set of resonant frequencies at which the performances are ruined.

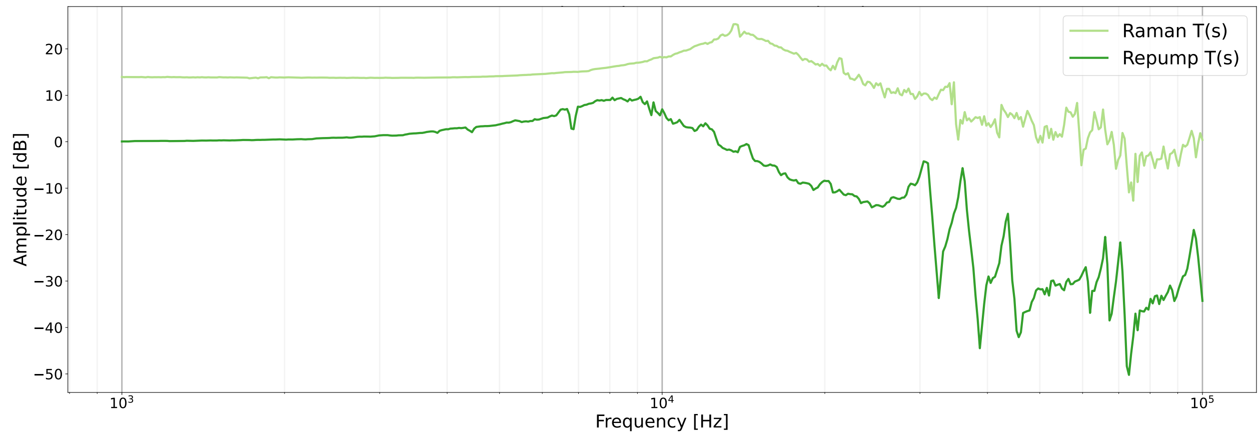

Figure 8: Servo bump comparison between Raman and Repump cavities. Note how the Raman cavity's one is shifted to higher frequencies, leading to higher bandwidth.

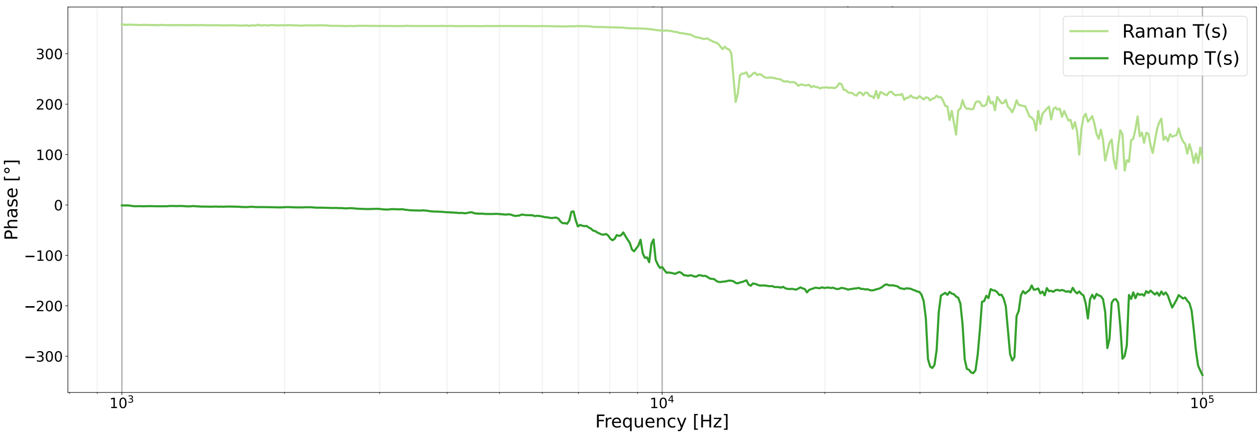

Figure 9: Resonances width comparison between Raman and Repump cavities. Broader resonances imply possible instability in response to a greater set of frequencies.

2.3 Acoustic noise characterization

Every object possesses its own mechanical resonance(s). Where in frequency they are located depends on different mechanical properties of the system such as mass, shape, density, Young modulus etc. In the doubling cavities, each single element have its natural resonance frequencies. When two or more objects are somehow coupled (for example, glued together), the resulting system shows eventually new resonant frequencies that depend both by the single object's ones and on the coupling mechanism. The box, the mirrors, the crystal and the piezo-actuated mirror system, are all more or less coupled and originate some mechanical resonances. Interesting would be to identify which components contribute the most to give rise to resonances that badly affect the cavity stability. Indeed, since one of the causes of instability of the cavities was high pitch sounds such as hand claps or vibrations coming from accidentally hitting the optical table, we further proceeded investigating how the systems respond when subject to acoustic noise at well defined frequencies. The setup we used, again took advantage of ADK's network analyzer function this time to drive a battery powered speaker at different frequencies via AUX connection. The schematic of the setup is presented in Fig. 10.

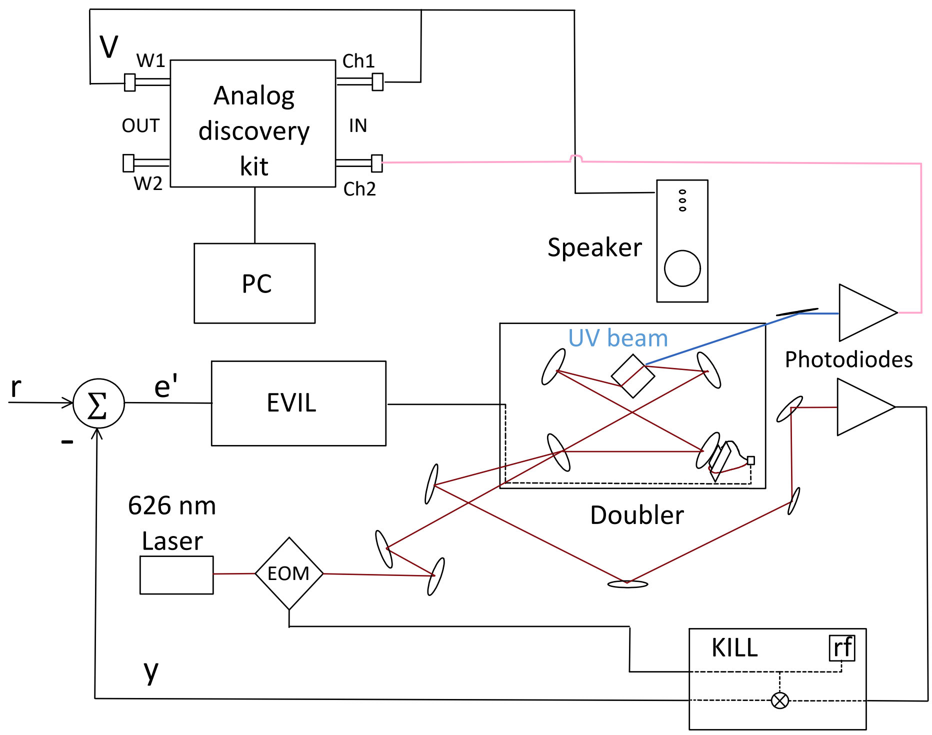

Figure 10: Acoustic noise characterization setup schematic. In this case the disturbance is coupled to the system via acoustic vibration. The noise frequency is controlled by ADK, which also analyzes the UV laser's response to it.

The speaker was suspended right above the doubling cavity at a distance of roughly 40 cm. Since the signal that requires stability is the UV generated laser beam out of the doubling cavity, we used it to characterize the noise response, as can be seen in the schematic.

2.3.1 Experimental results

After having found a workable amplitude to generate a rather intense sound, we obtained the data for all the cavities, separately reported in Appendix B and grouped in two couples in Figs. 11 and 12, where the plots have been offset for clarity. In the graphs, the range o frequencies is limited to 100 Hz - 25 kHz ,since the speaker's bandwidth is 65 Hz - 20 kHz. The signal we were looking at comes from a photodiode and is then delivered to the ADK. The resulting plot represents the system's response at a particular frequency, given the noise being at the same frequency. Acoustic noise directly affects the output laser beam's power spectral density. Therefore peaks as the one in Fig. 11 indicate mechanical resonances of the system at these specific frequencies. The acoustic noise characterization was performed for all the Molecules' and Penning's doubling cavities.

Analyzing the data, besides a positive slope shared by all the responses, we can in general state that:

- Molecules' cavities show a similar behaviour, for example sharing a resonance around 700 Hz and two of what at first sight may seem "resonance bumps" from 1 kHz and 2 kHz and around 10 kHz.
- Penning's cavities also share similar behaviour concerning the resonance bumps. Nevertheless, while the Detection cavity shows more numerous higher resonances from 1 kHz

to 4 kHz, the Repump cavity exhibits two pronounced peaks at 340 Hz and 1.5 kHz. Another common feature is again a resonance bump centered at 7 kHz.

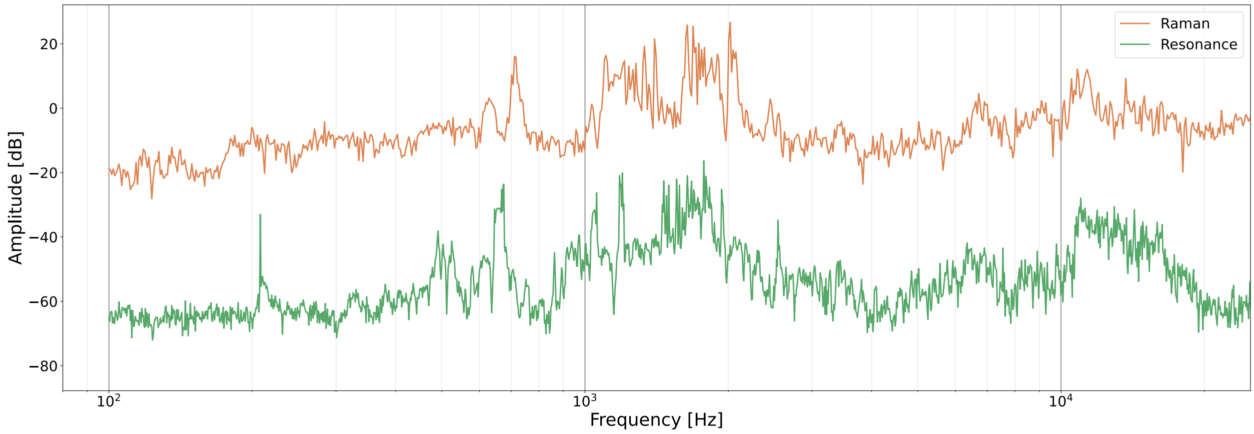

Figure 11: Acoustic Noise response in Raman and Resonance cavities

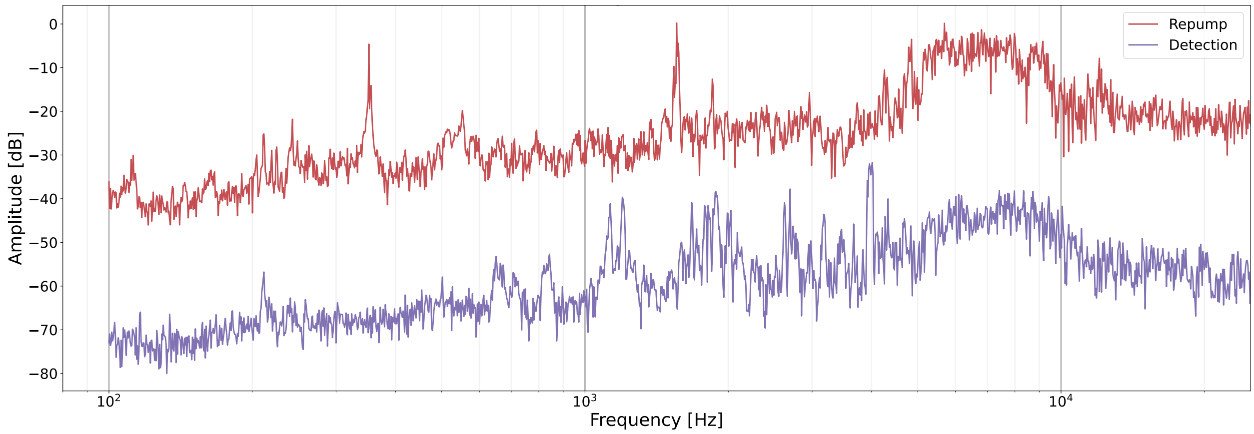

Figure 12: Acoustic Noise response in Repump and Detection cavities

To understand from which cavity one should expect more disturbance insensitivity, it is necessary to point out that the most common acoustic vibrations in the lab derive either from human voice or from the sound made while accidentally hitting something (example: laser safety barriers). Human voice typically consists of sound waves in the range 80 - 265 Hz, while all the other noises can have different spectra. As a reference, we can pick a hand-clap as an example, since direct observation of instability has been observed in response to that. A hand-clap spectral density has been shown [14] to have roughly flat distribution in the range 200 Hz - 6 kHz or even being peaked from 200 Hz to 1 kHz depending on the clapping "method". Molecules' doubling cavities indeed were observed to be more susceptible to the hand-clap kind of noise, in agreement with the higher resonance bump observed from 1 to 2 kHz, absent in the Resonance cavity and lower in the Detection one. Furthermore, we proceeded investigating the effect that modifying some coupling mechanisms within one of the cavities setup has on the noise response. In particular, we tested the removal of the Plexiglas cover in Raman cavity. We did so because we expected the cover to partially isolate the cavity from acoustic noise. As can be seen from Figure 13, the effect of it is almost negligible at lower frequencies, while for high frequencies some effects are recognizable. First, the dip at 1.4 kHz in "normal" configuration is eliminated by removing the cover. Moreover, a resonance at 2.5 kHz becomes much more pronounced, and the high frequency response is in general higher, meaning more sensitivity to noise and worst performances, as discussed. Our hypotheses was therefore confirmed.

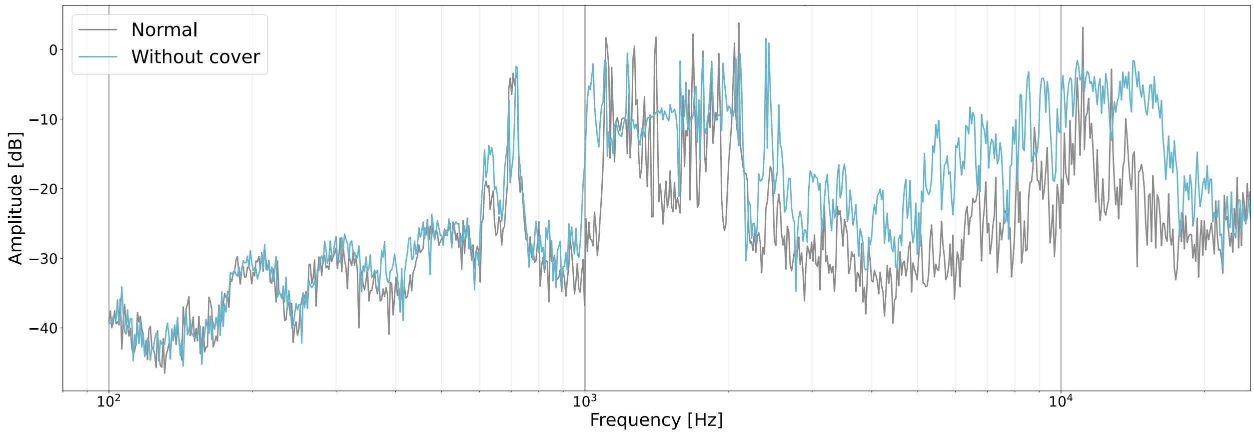

Figure 13: Acoustic Noise response in Raman Cavity with and without cover. Low frequency behaviour is the same, high frequency response gets worse without the cover, as expected.

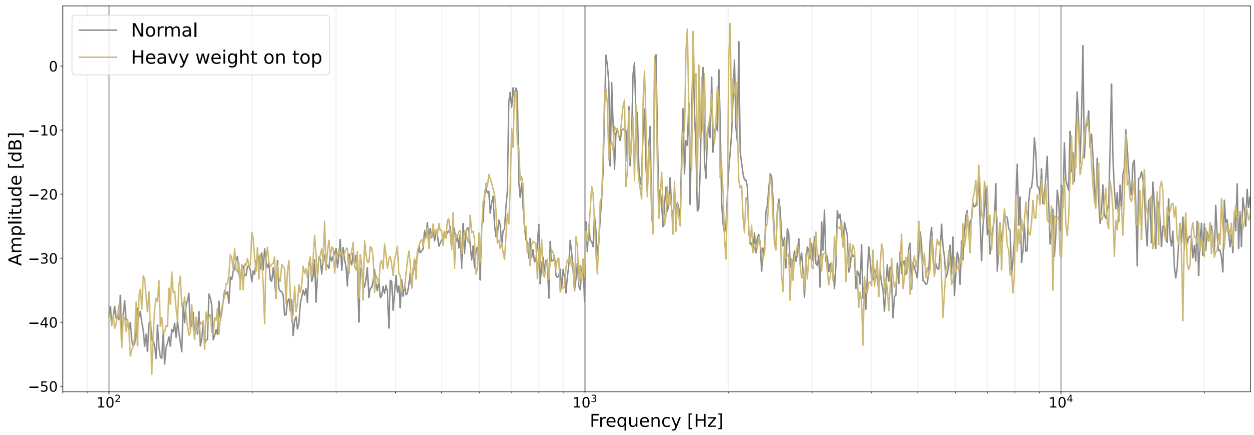

Figure 14: Acoustic Noise response in Raman Cavity with and without a weight put on top. No differences are observed.

Negligible results were obtained if a heavy weight was put on top of the covered cavity, as can be seen in Fig. 14. That was expected to change the overall coupling to acoustic modes, but we did not expect any particular behaviour.

Lastly,the comparison between acoustic noise response and the amplitude response of the respective complementary sensitivity function $T(s)$, allows us to partly explain some features in the acoustic noise response behaviour of the cavity.

As can be seen in Fig. 15 and the last two pictures at the end of appendix B, those that could be interpreted as ”bumps” due to a set of neighbor resonant frequencies from 1 kHz to 2 kHz, could be related con the servo bump of the electrical response. This may somehow be explained by the fact that electrical and mechanical resonances in the piezoelectric chip are necessarily linked due to the piezoelectric property. On the other hand, it’s true that no phase shift is observed at the servo bump frequencies.

3 Mechanical resonances in the mirror-piezo-mount system

After having characterized the doubling cavities’ noise response, we moved to analyzing one source of resonances in the system, namely, the piezo-actuated mirror. When used in a closed loop configuration, the bandwidth of piezo actuators is often limited by strong mechanical

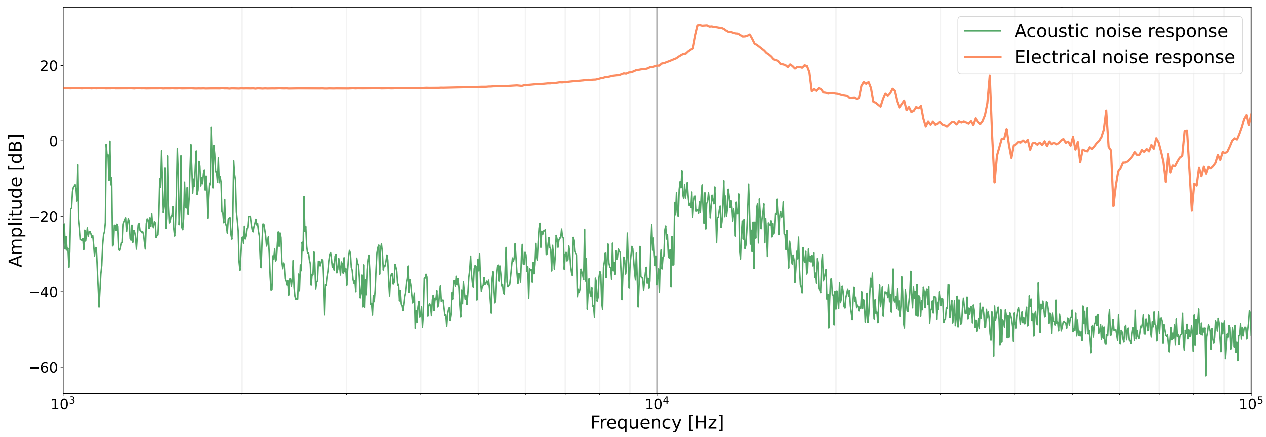

Figure 15: Electrical and acoustic noise response comparison in Resonance cavity

resonances between 20 and 40 kHz [15],[16]. These resonances are problematic, because of the strong phase shifts they cause, which in turn can lead to positive feedback and therefore instability of the cavity lock.

3.1 Piezo-actuated mirror design

One part of the project was dedicated to understanding if and how different components of the MPM system may be related to each other in order to possibly push the natural resonances further in frequency thus allowing for a higher bandwidth.
The MPM system is simply built as follows. The piezo-chip is glued to the mounting structure on one side and to the dielectric mirror to the other. As comes from previous work from [17], each component must be properly chosen to maximize the resonant frequency while at the same time minimizing the quality factor of mechanical resonances. Since we have a specific required mirror type for the doubling cavity (different from the one used in our characterization), we focused on the choice of the piezo-actuator, the adhesive and the mount shape and realization. First, let's investigate the shape of the mounting structure. As a first remark, one should recall that a material's stiffness (often measured by the Young's modulus) is proportional to its mechanical resonance frequency [18]. A schematic of our mounting structure is presented in Fig. 16. Here, the external orange cylinder and the blue inner one are made of steel, while the middle green one is made of lead. The latter, thanks to its higher density, but lower Young's modulus, should act as a damper for steel's mechanical resonances, as suggested in [17], therefore lowering their intensities. The sizes of the three cylinders are reported in Table 1.

Cylinder	**Diameter [mm]**	**Height [mm]**
Outer	25	12.5
Medium	22.5	12.5
Inner	9	N.A.

Table 1: Sizes of mounting structures parts.

Concerning the choice of the piezoelectric chip, we decided to use two different ones. The first choice was to use the same present in the doubling cavity, with the goal of create a system that somehow replicates the MPM used in the doubling cavities (except for the mirror). The second served as a prototype for future replacement of design in case of improvement. Their most important features are compared in Table 2. Both the chips are manufactured by Thorlabs.

The choice of switching from a rectangular- to round-shaped chip is made to reduce the

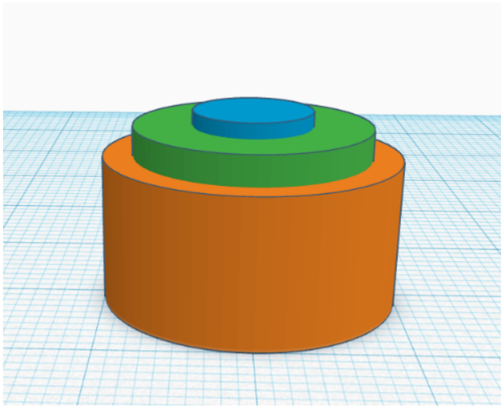

Figure 16: Mounting structure designed for the the MPM system. The orange and blue cylinders are made of steel, the green one is lead.

Code	Label	Cross section	Res. Frequency[a] [kHz]	Capacitance [nF]
AE0203D04[b]	Old	Rectangular	261	90
PA25FEW	New	Round	350	150

Table 2: Comparison of the piezoelectric chips' relevant properties.

[a] Unloaded.
[b] No longer available for purchase.

effect of drum-head modes via matching the shape of the mount and the dielectric mirror [17]. In principle, one would also prefer size matching at the interface, but this was not possible due to the constraint on the mounting structure. Moreover, the second piezo-chip's unloaded resonance frequency is higher.
The rationale for the choice of the glue comes from modelling the mount-piezo-mirror system as coupled harmonic oscillators [17], in which the glue represents the springs. The resonance frequencies of the whole system can be pushed higher by making sure that the "spring constant" parameter k is sufficiently high. Thinking of the glue layer as a bar being compressed, we can model the constant as:

$$k = \frac{EA}{L} \tag{7}$$

where E is the Young's Modulus, a measure of stiffness, L is the bar's length and A is its cross sectional area. To make k as big as possible, we applied a set of procedures fruitful in [17].
First, we applied pressure according to the data-sheet of the chosen bonding agent to reduce the layer thickness L and we chose Crystalbond M-Bond 610 adhesive agent (which is typically used for strain gauges application and was suggested in [17]) that among our options constituted the optimal solution for our purpose and at the same time presented a sufficiently high viscosity for the rigidity needed to enhance the Young's modulus E. In order to maximize A, we made sure to apply the adhesive to the whole surfaces of the piezo, the mirror and the mount structure. One remark regarding the differences among gluing process with M-Bond 610 and the Araldit 5 minutes epoxy is that the first requires high temperature curing for an amount of time in the hours range, depending on the specific temperature, while the latter is a more general purpose glue, fast curing at room temperature. In both case pressure was applied only when gluing the piezo to the mounting structure, avoiding it when attaching it to the mirror because of the risk of scratching it.
In the following we will label the three different systems we characterized as follows:

- S1 = Mount, Thorlabs Rectangular Piezo Chip AE0203D04, Thorlabs dielectric mirror BB03-E02, Araldit 5 minutes epoxy.

- S2 = Mount, Thorlabs Rectangular Piezo Chip AE0203D04, Thorlabs dielectric mirror BB03-E02, Adhesive agent M-Bond 610.
- S3 = Mount, Thorlabs Round Piezo Chip PA25FEW, Thorlabs dielectric mirror BB03-E02, Adhesive agent M-Bond 610.

In Fig.17, pictures of S1 and S3 are shown. Note that S1 and S2 look the same, since only the glue changes.

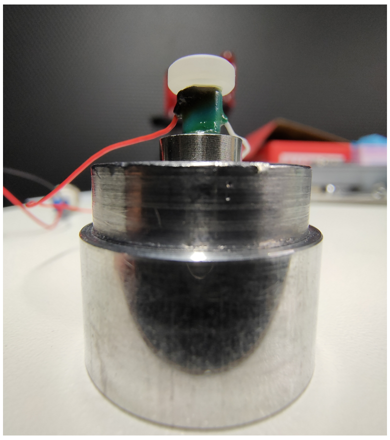

(a) S1.

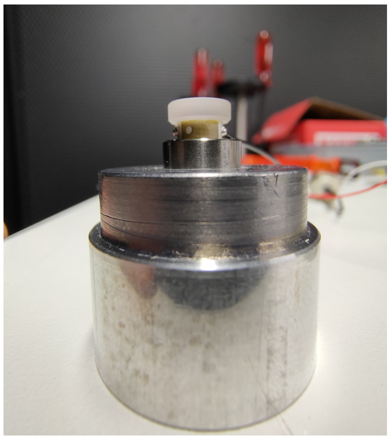

(b) S3.

Figure 17: Picture of two out of three characterized systems. S1 and S2 both look like in (a).

3.2 Resonances measured via Michelson interferometer

3.2.1 General theory

A Michelson interferometer is an optical setup used to observe phase variation in a laser beam related to a physical phenomenon of interest. An incoming laser beam is split in two secondary beams with a (typically 50:50) beam splitter. These two go in two separate arms, where from one side, the so called reference beam travels a fixed path length, while in the other arm the beam undergoes a phase shift. The signal of interest then is the interference given by the two beams being recombined and overlapped. A picture of our Michelson interferometer is shown in Fig. 18.

The scheme of the optical setup and the electronic equipment is shown in Fig. 19.
We use a 632.8 nm, 5 mW He-Ne laser [Thorlabs HNL008L] with a coherence length of $l_{coh} \simeq 30$ cm, which is sent through a polarization filter and then impinges onto a polarizing beam-splitter, which happened to already be built in the setup, but had no purpose in our experiment. Then, the beam travels through another 50:50 non-polarizing beam-splitter, which creates the two beams that go in the two arms. The first one is the reference beam (r) to the left in Fig. 19, while the other (p) goes through the second arm and gets phase shifted. The phase shift happens due to difference optical path, and can be controlled by the piezo-actuated mirror. Finally, the signals are recombined at the beam splitter and the interference signal is captured by a photodiode. The piezo element is driven by a self-built instrument containing a high voltage ultra low noise piezo-driver [PDu150] [19]. Its three channels were first wired into one to obtain higher output power. This, amplifies the input signal generated by the Analog Discovery 2 Kit with a 40 V offset and a gain of $G = 20$.

Before proceeding with the actual experiment, we looked at the interference signal, adjusting the setup to properly align the beams. When the piezoelectric element is turned off, the two beams have a certain phase difference that is simply given by the different optical path lengths. The exact path difference is, however, not relevant for the following. Only the phase difference matters. Once the driving signal is turned on, the piezo-chip moves the

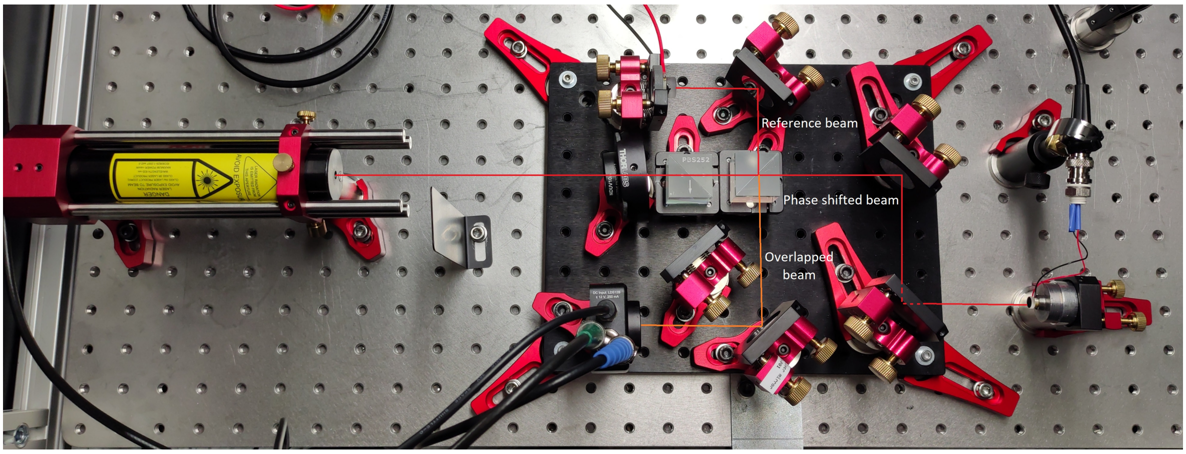

Figure 18: Michelson interferometer used in the characterization. Reference beam is in the upper part, the phase phase shifted one is in the right arm. The two are recombined at the non-polarizing beam splitter and reflected to the photodiode. Non relevant beam reflections are not drawn.

mirror, thus modifying the path length of the beam. We therefore observe a change in the interference signal. We define $\Delta L = |L_1 - L_2|$ to be the optical path difference. The change in interference signal as the mirror gets shifted happens because of constructive or destructive interference at the photo detector. These correspond respectively to:

$$\Delta L = k\lambda, \quad \text{with} \quad k \in \mathbf{N}.$$
$$\Delta L = \frac{(2k+1)}{2}\lambda, \quad \text{with} \quad k \in \mathbf{N}.$$

In this preliminary step, one needs to obtain a very good overlap of the beams performing a beam walk to obtain increase the interference signal's SNR. Moreover, as a technical remark, in the Michelson's setup, it is fundamental to make sure that the coherence length of the laser is greater than the maximum difference between the optical path lengths in the two arms, namely: $l_{coh} \geq \Delta L$ [20].

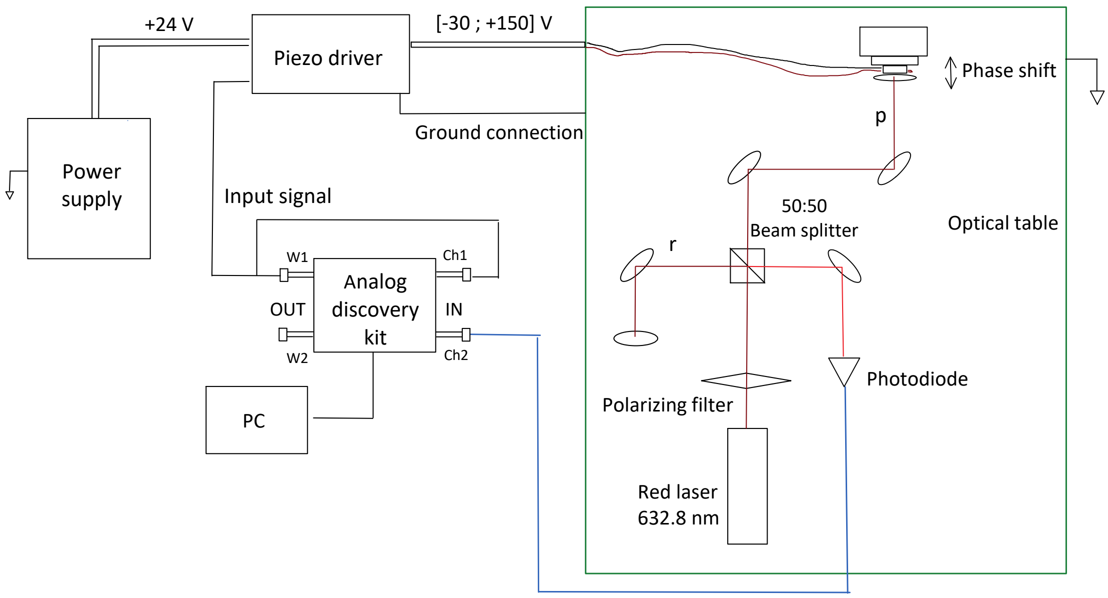

Figure 19: Schematic of our Michelson interferometer setup. The ADK delivers the driving signal via W1 that gets amplified and sent to the piezoelectric element. ADK also analyzes the interference signal coming from the photodetector via Ch2.

3.2.2 Experimental results and comparison with noise response

After having set up each system, we needed to make sure that certain conditions were satisfied:

- The p beam must be self-overlapped before and after hitting the piezo-actuated mirror, meaning it must hit the mirror at 90°.
- r and p must be well overlapped when mixed. One should also be careful to have the r beam self-overlapped as well. This can be made better by beam walking the reference beam until a nice interference pattern is observed.
- The overlapped signals have to be well centered to the photodetector's sensor.

If this procedure is successfully completed, the interference signal obtained ramping up the piezo drive should look as shown in Fig. 20.

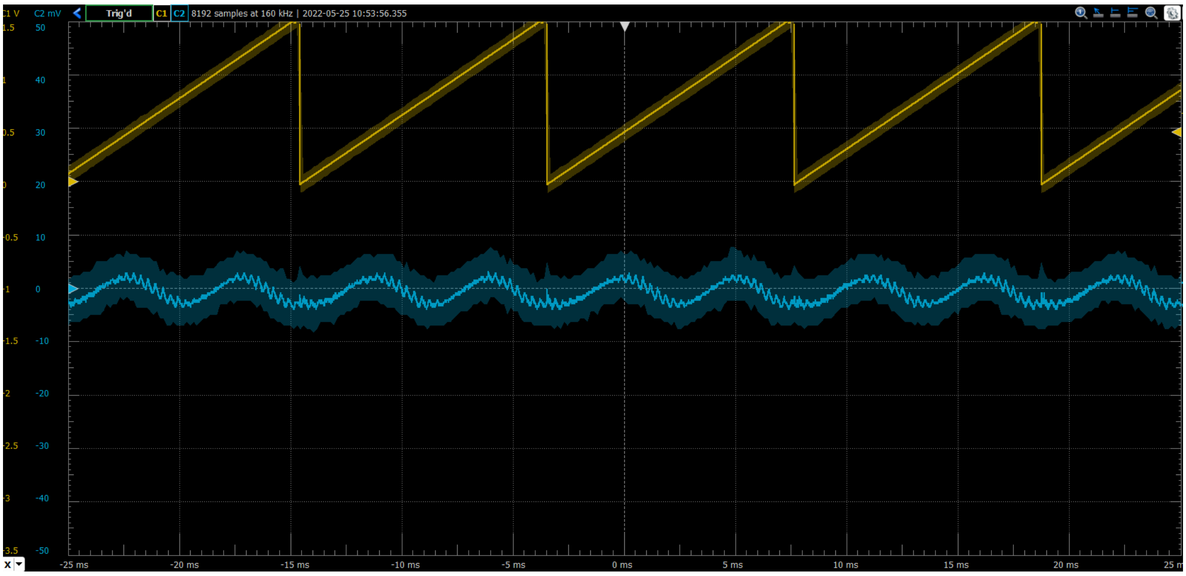

Figure 20: Interference (in blue) and piezo driver input (yellow) signals observed via Waveforms GUI.

The origin of the higher frequency noise has never unequivocally been qualified, but the most probable hypotheses relies on some intrinsic noise in the laser, since over many repetition of the experiment we were never able to eliminate it completely. Regardless, the measurement of the resonances should not have been affected, since what we are interested in is the response at each frequency component, so additional noise in the laser at a certain frequency does not affect all the others. Once we had the interference signal for a certain run of the experiment, we could choose a DC offset for the following part so that we sit at one of the inflection points of the interference signal, where the slope is maximum. In this way as we slightly changed the drive voltage adding a small amplitude AC probe signal, it resulted in the maximum deviation from the offset point. This is particularly useful to obtain a nice contrast when a resonance frequency is hit. To implement this kind of measurement, we switched to the network analyzer function of the ADK to generate a 10 mV (lowest amplitude possible) signal sweeping the frequency, superimposed to a DC offset.
The characterization of the systems in Fig. 17 and above described showed to be repeatable over different run of the experiments and different ranges of frequencies evaluated. The results for the three systems probed in the range 600 Hz - 150 kHz is reported in Figs. 21, 22, 23.
Some observations can be made on these data. The change of the glue seems to have systematically shifted the resonant frequencies of 8-10 kHz. It is important to note though, that measurement of S1 have been done after having come apart S2 via heating. For this reason, it cannot be excluded that the piezo-chip has been affected in the procedure. To ensure the

reliability of these data, one should build a replica of S1 with an unused piezo element or detach the piezo-chip from S1 to rebuild S2. The first option was not viable due the lack of old piezo-chip samples (they are out of production). The second was not followed due to time constraints. It will pursued after the end of this project.
Comparing Fig. 23 with the previous two, one can conclude that the change of the piezo-chip basically left the lower resonances unchanged, while it seemed to have shifted to the left the higher frequencies one. Assuming the glue to have benefited to the system, these last result seems to disprove the hypotheses made on the better compatibility due to the piezo-mirror shape-matching. Nevertheless, in [17], the mismatch between the mirror and the piezo element was smaller than ours, and they further manipulated the piezo-chip. In particular, their goal was to push the resonance frequencies to higher values while at the same time reducing their quality factor Q. To o so, they roughened of of the surfaces of the piezo element by cutting it parallel to the surface with a diamond-saw. These two caveats may be part of the reason for our different findings, even though the surface roughing only led them to attenuate resonances at higher frequencies ($\geq$ 100 kHz) . Damping of lower frequencies resonances was obtained with a bullet-like shape of the mount. For this reason, it is possible that the low frequencies resonances that we still observe and that got even worse are due to the mount, and that switching the piezo had just shifted them to lower frequencies due to the mechanical coupling (different mass), although the piezo-chip itself may show better performances at higher frequencies.

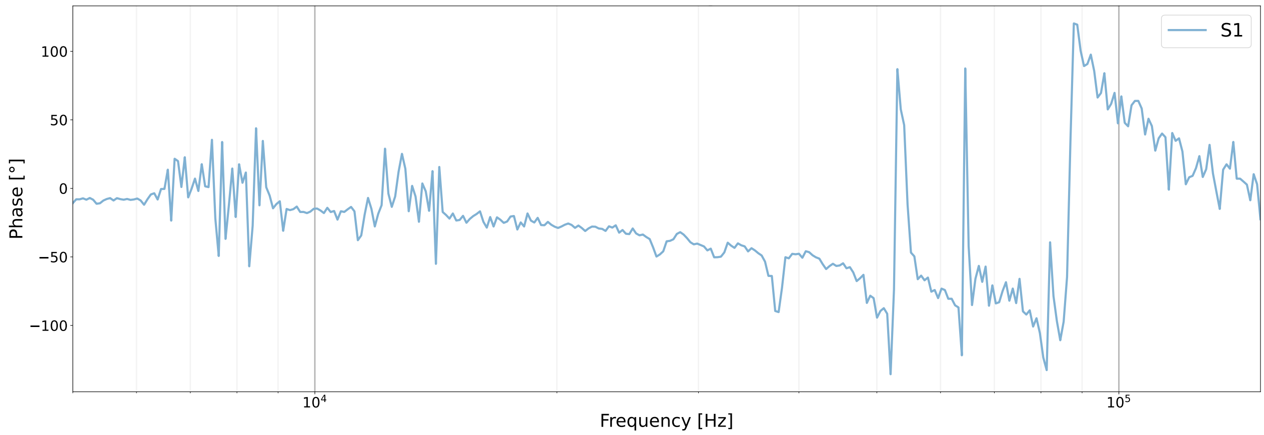

Figure 21: S1 system's interference signal in the Michelson's setup

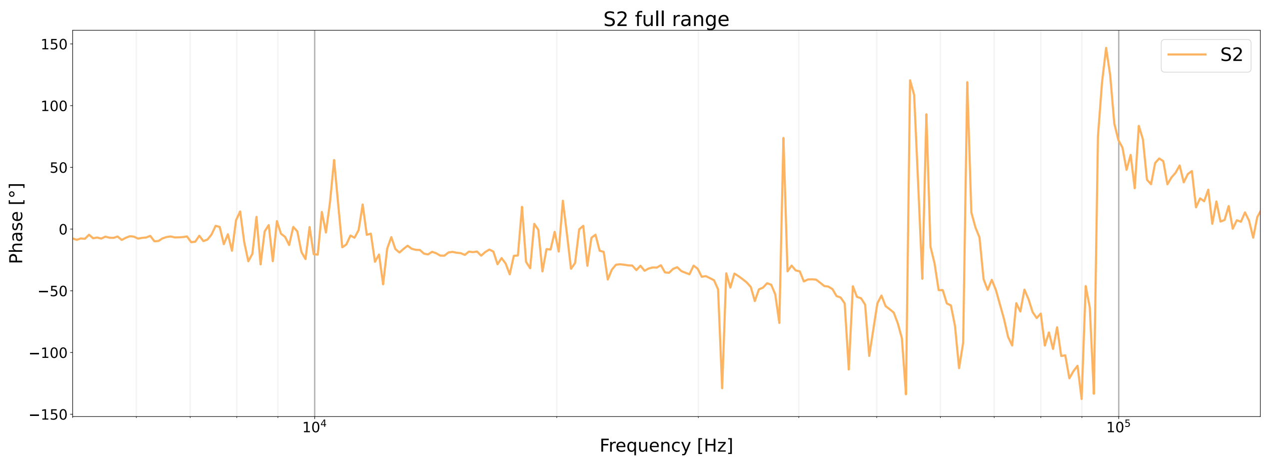

Figure 22: S2 system's interference signal in the Michelson's setup

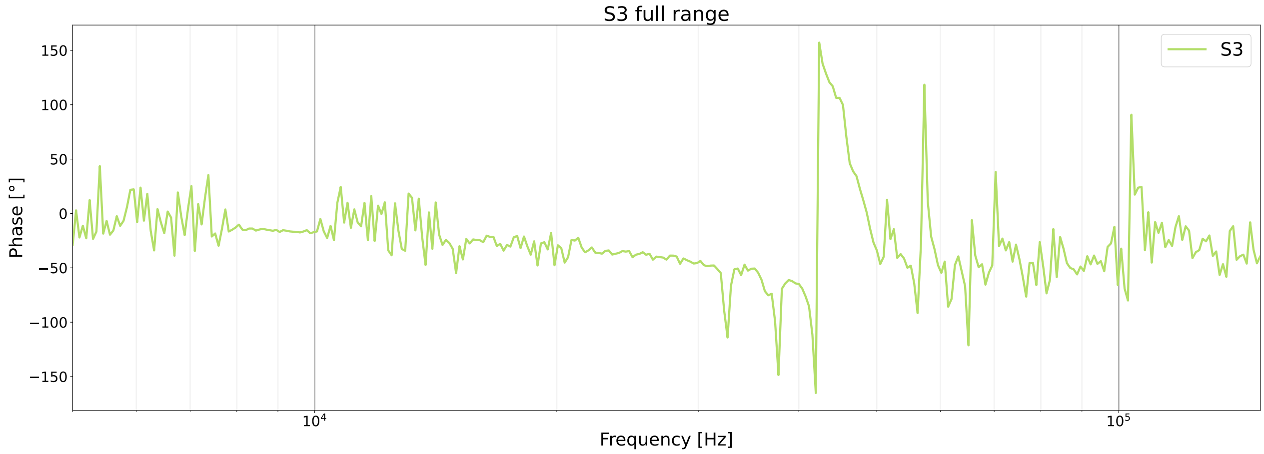

Figure 23: S3 system's interference signal in the Michelson's setup

To conclude this investigation, one can compare these measurements and electric noise response measurements on the doubling cavities. The comparison with the acoustic noise was attempted, but the small overlap of frequencies ranges between the two did not lead to anything noticeable and has been therefore disregarded. The small overlap comes from the difference investigation range of the two measurements. The speaker's bandwidth is limited to 20 kHz, while in the Michelson experiment was run until 150 kHz. The electrical noise comparison with the Michelson's data is presented in Fig. 24.

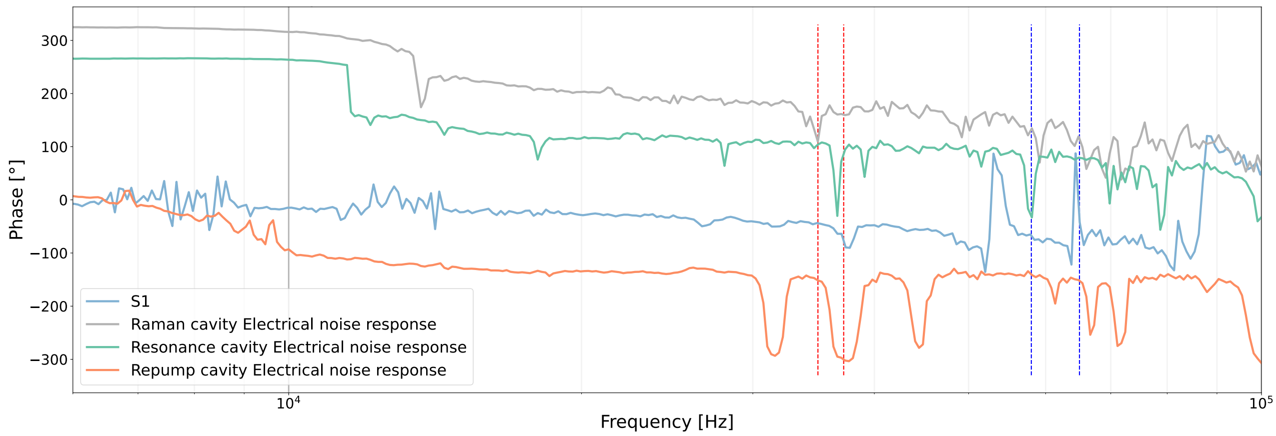

Figure 24: Comparison Michelson's measurements-electrical noise response. The single plots have been offset for clarity.

Before looking closely at the data, one should recall that the mirror mounted in the doubling cavities is different from the one used in S1 (indeed, bigger), so it is not so easy to draw conclusions.

We cannot see a lot of resonant frequencies matching, but we could identify some correlations among them. For example, the dip at 37 kHz in the S1's Michelson response corresponds to a resonance in both the Repump and the Raman cavities, while in the Resonance cavity, a resonance at 35 kHz can be observed (red dashed lines). Less remarkable is the correspondence at higher frequencies (blue dashed lines) where the Raman and Resonance cavities share a resonance at around 58 kHz, that may be related to the peak in the S1 system response and the set of resonances around 65 kHz. In general, it is clear that the coupling of the piezo-actuated mirror with the rest of the cavity has shifted the resonances, but probably not in a systematic way. This is probably due to two factors, the first being possible construction differences in the cavities and second relying in the different mirror used in the doubling cavities and in S1.

4 Conclusion and further work

The goal of the project was to characterize the doubling cavities' electrical and acoustic noise response after their instability to acoustic noise was observed. In second place, some alternatives for the MPM system were investigated.

The electrical noise characterization led us to observe that the sensitivity and complementary sensitivity functions, although reasonably following the ideal behaviour, show marked electrical resonances, especially in $T(s)$. The higher frequency servo bump observed in the Molecule's doubling cavities suggests them to have a better behaviour in a noiseless environment. Nevertheless, the acoustic noise response characterization confirms Penning's cavities higher robustness against acoustic noise. In fact, those plots shows that their response is flatter than Molecules' in the range 1 kHz - 10 kHz, where much of the acoustic noise in the lab is focused. The resonances bump in the range 5 kHz - 10 kHz in Fig. 12 was shown to be correlated to the electrical one and not implying any phase instability.

The analysis of Fig. 13 indicates the covering of the cavity to improve the system performances at frequencies higher than 1 kHz. This suggests that one possible approach to better the system could be inserting some laser safe sound absorbing foam inside or outside the cover. Lastly, the measurements with the Michelson interferometer suggest that the change of the adhesive for the MPM system could be helpful to shift mechanical resonances in frequency. On the other hand, further confirm of it is necessary, as previously discussed. The change of shape of the piezo is apparently not sufficient to improve the system's performance, rather, in this case it led to worst results. Modifying the piezo element and mounting structure as discussed may be a valid direction to continue this project. The difficulty in comparing the results from S1 to the cavities' noise responses also suggests to consider repeating the Michelson interferometer experiment with the same mirror present in the cavities.

A Electrical noise characterization - graphs

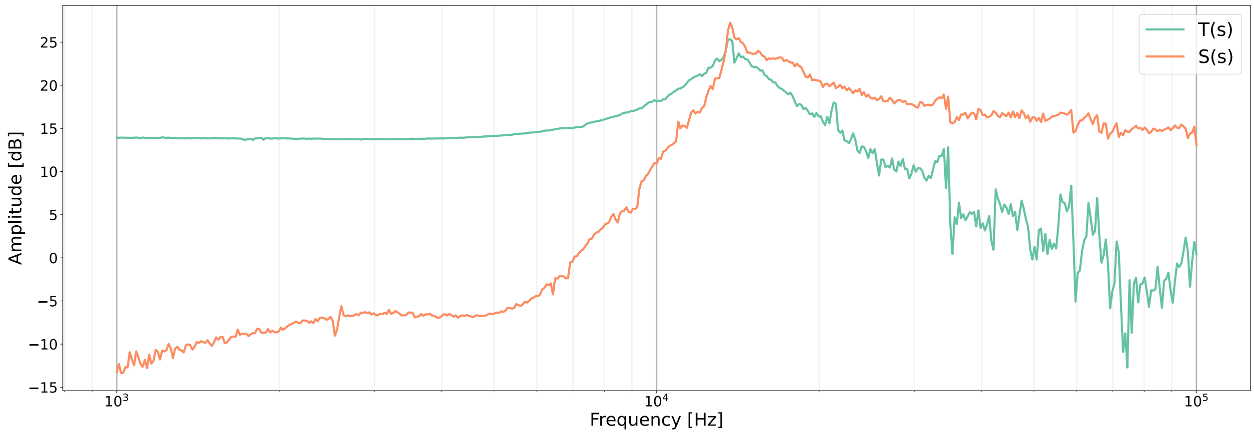

Figure 25: T and S amplitude response of the Raman Cavity

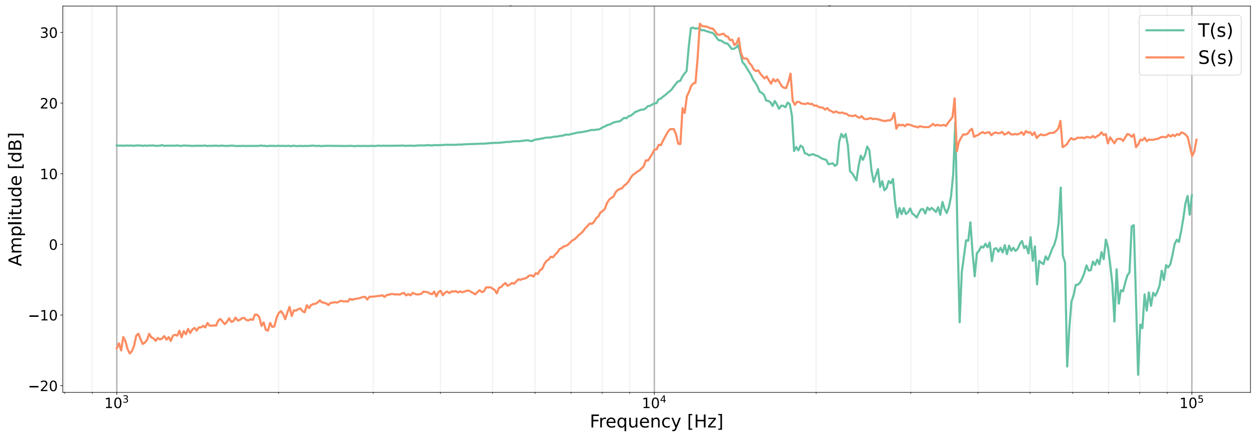

Figure 26: T and S amplitude response of the Resonance Cavity

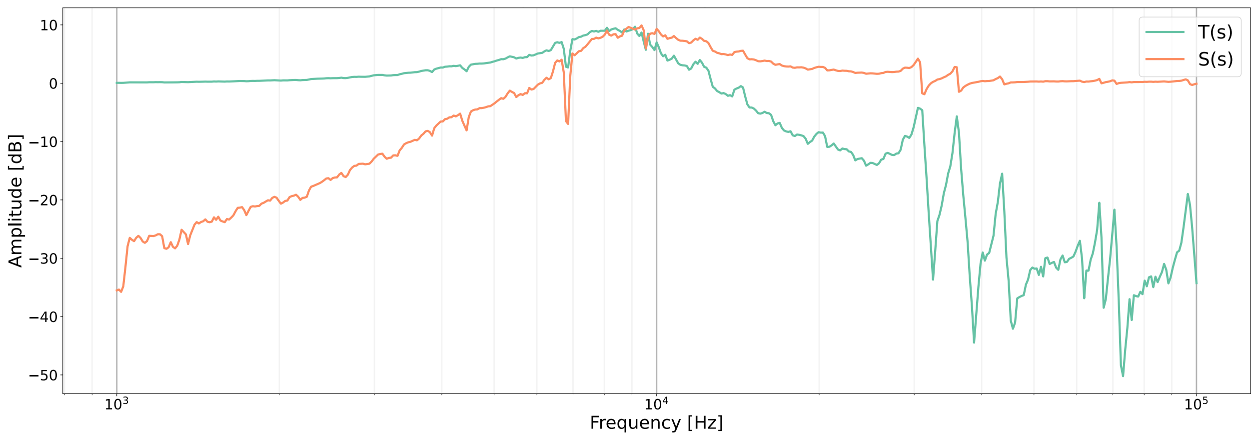

Figure 27: T and S amplitude response of the Repump Cavity

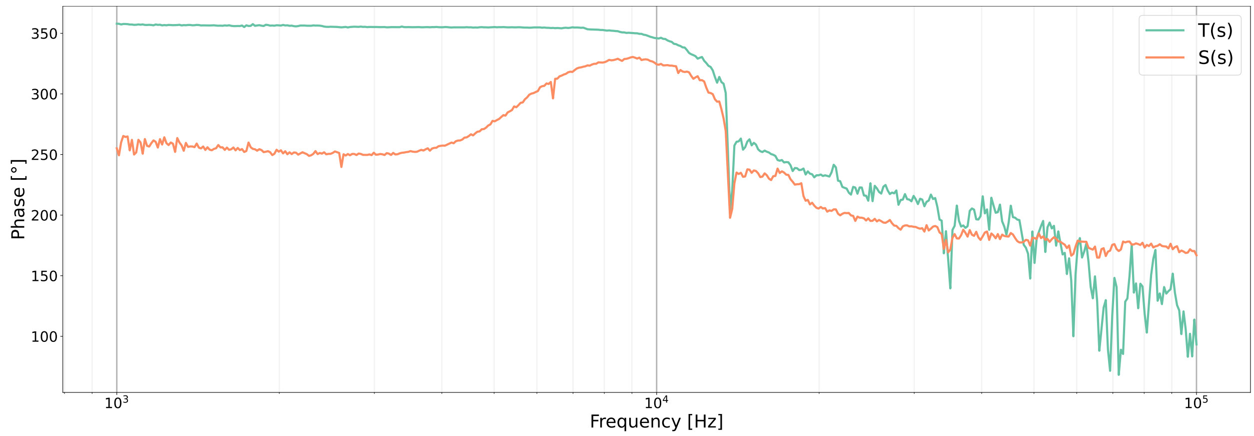

Figure 28: T and S phase response of the Raman Cavity

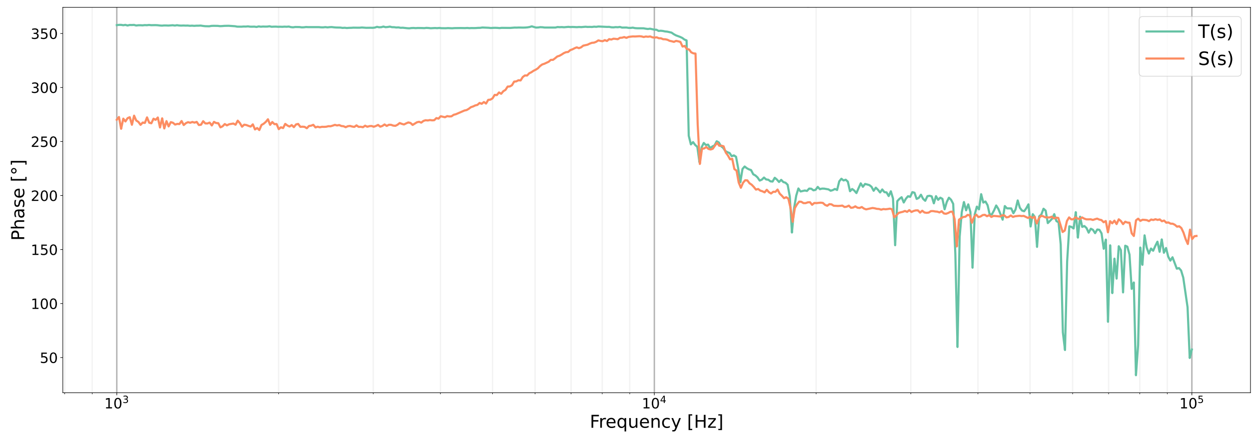

Figure 29: T and S phase response of the Resonance Cavity

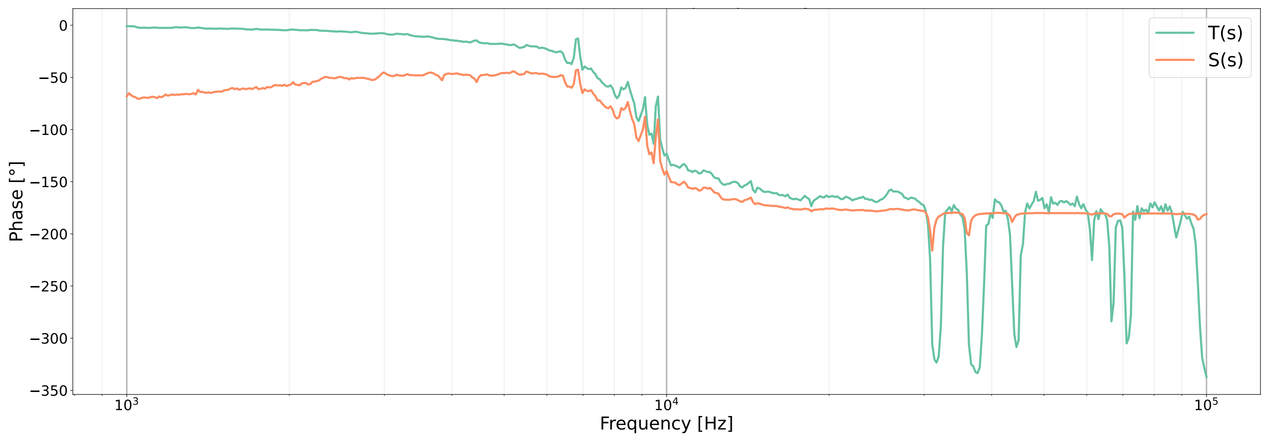

Figure 30: T and S phase response of the Repump Cavity

B Acoustic noise characterization - graphs

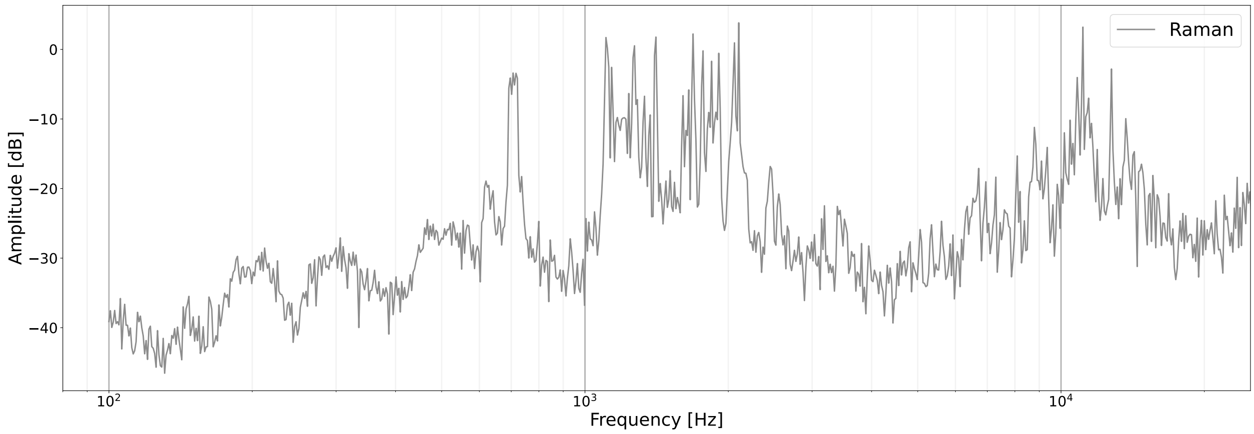

Figure 31: Acoustic Noise response in Raman Cavity

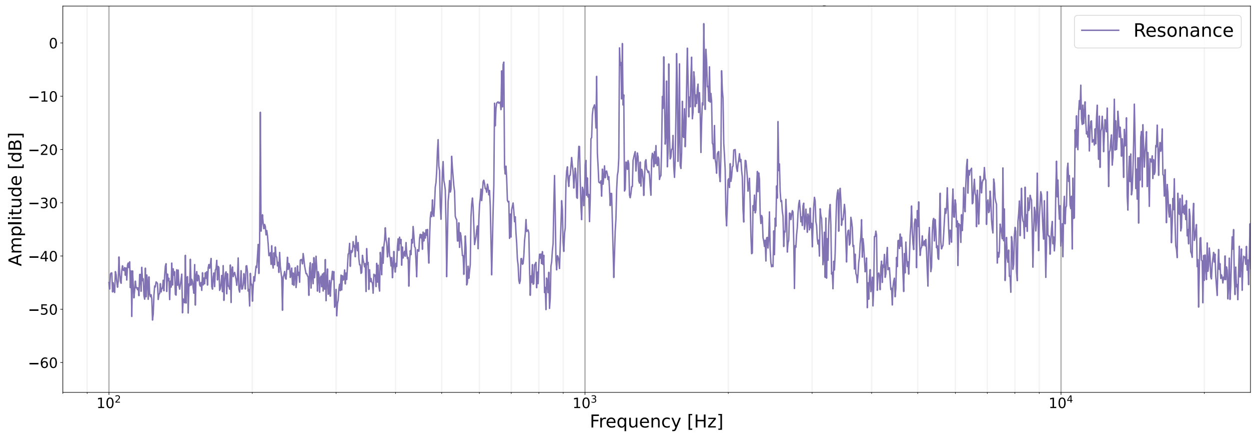

Figure 32: Acoustic Noise response in Resonance Cavity

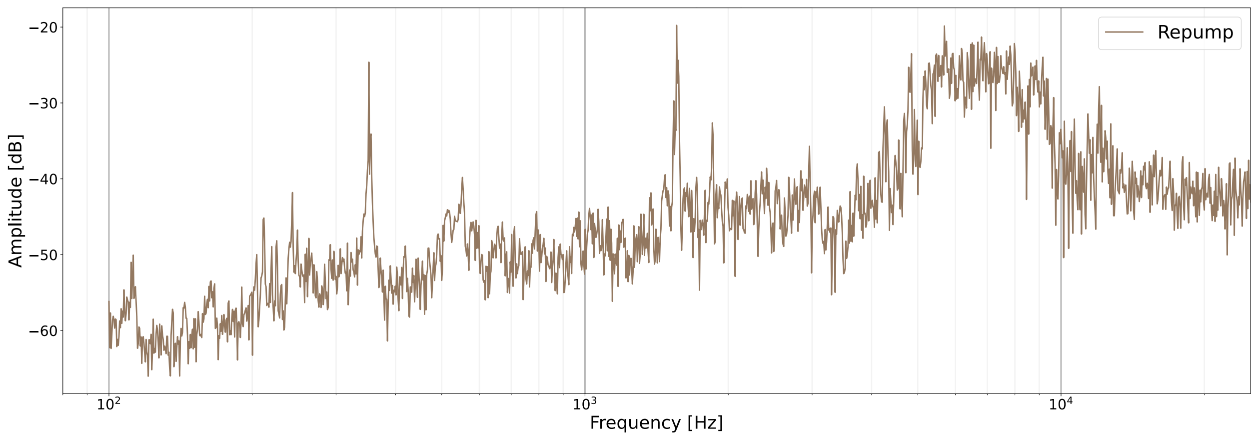

Figure 33: Acoustic Noise response in Repump Cavity

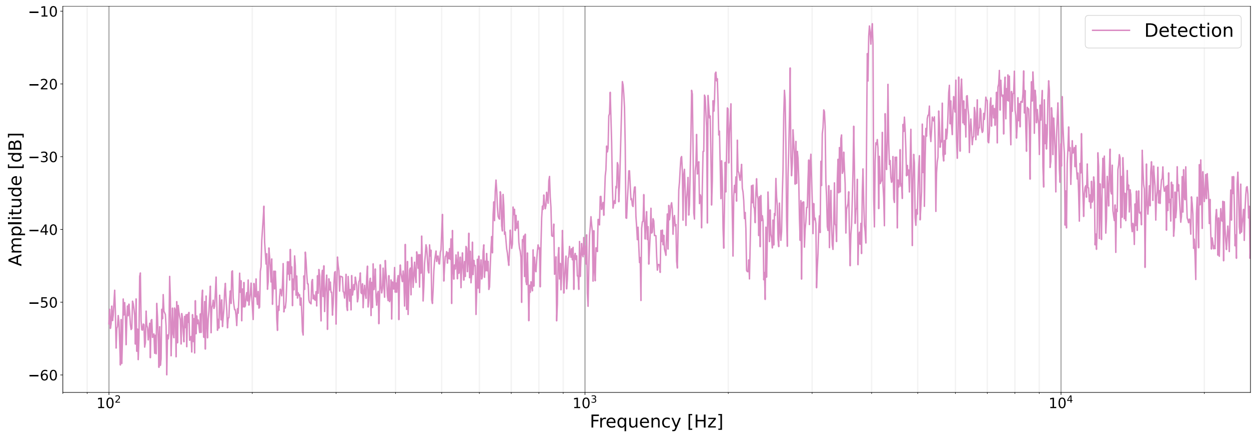

Figure 34: Acoustic Noise response in Detection Cavity

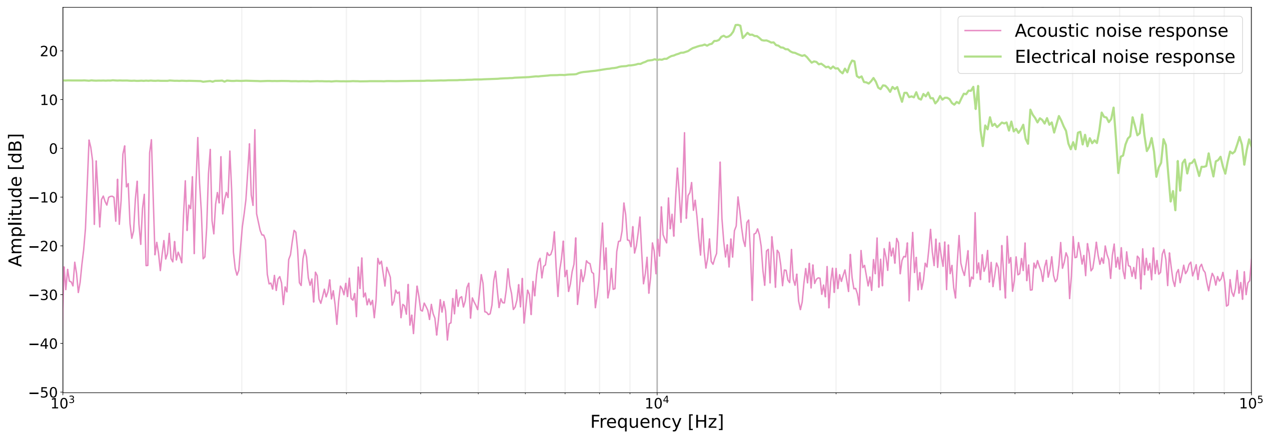

Figure 35: Electrical and acoustic noise response comparison in Raman cavity

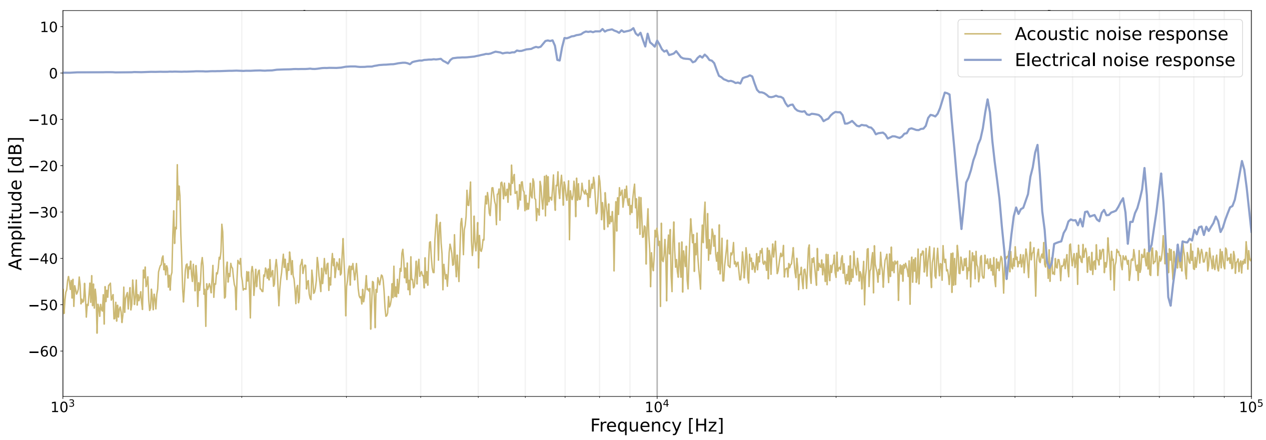

Figure 36: Electrical and acoustic noise response comparison in Repump cavity

References

[1] D. A. Kleinman, “Theory of second harmonic generation of light,” *Physical Review*, vol. 128, no. 4, p. 1761, 1962.

[2] V. Berger, “Second-harmonic generation in monolithic cavities,” *JOSA B*, vol. 14, no. 6, pp. 1351–1360, 1997.

[3] “Tiqi-molecules page.” (), [Online]. Available: `https://tiqi.ethz.ch/research/molecules.html`.

[4] R. Drever, J. L. Hall, F. Kowalski, *et al.*, “Laser phase and frequency stabilization using an optical resonator,” *Applied Physics B*, vol. 31, no. 2, pp. 97–105, 1983.

[5] M. G. Cain and M. Stewart, “Piezoelectric resonance,” in *Characterisation of Ferroelectric Bulk Materials and Thin Films*, M. G. Cain, Ed. Dordrecht: Springer Netherlands, 2014, pp. 15–35, ISBN: 978-1-4020-9311-1. DOI: `10.1007/978-1-4020-9311-1_2`. [Online]. Available: `https://doi.org/10.1007/978-1-4020-9311-1_2`.

[6] E. D. Black, “An introduction to pound–drever–hall laser frequency stabilization,” *American journal of physics*, vol. 69, no. 1, pp. 79–87, 2001.

[7] A. Haase, “Single atom detection in low finesse cavities,” Ph.D. dissertation, Jun. 2005.

[8] J. Capmany and C. R. Fernández-Pousa, “Quantum modelling of electro-optic modulators,” *Laser & Photonics Reviews*, vol. 5, no. 6, pp. 750–772, 2011.

[9] B. Keitch, “A quantum memory qubit in calcium-43,” Ph.D. dissertation, PhD thesis, University of Oxford, 2007.(cited on pages 30, 42), 2007.

[10] G. F. Franklin, J. D. Powell, A. Emami-Naeini, and J. D. Powell, *Feedback control of dynamic systems*. Prentice hall Upper Saddle River, 2002, vol. 4, ch. 6.

[11] F. Dörfler, *Closed-Loop Stability Criteria: board notes of the class "Control Systems I"*. 2021.

[12] “Digilent website: Analog discovery kit 2.” (), [Online]. Available: `https://digilent.com/shop/analog-discovery-2-100ms-s-usb-oscilloscope-logic-analyzer-and-variable-power-supply/`.

[13] “New focus website: Lb1005 servo controller.” (), [Online]. Available: `https://www.newport.com/p/LB1005-S`.

[14] N. H. Fletcher, “Shock waves and the sound of a hand-clap–a simple model,” *Acoust. Aust*, vol. 41, pp. 165–168, 2013.

[15] J. Debs, N. Robins, A. Lance, M. Kruger, and J. Close, “Piezo-locking a diode laser with saturated absorption spectroscopy,” *Applied optics*, vol. 47, no. 28, pp. 5163–5166, 2008.

[16] W. P. Bowen, “Experiments towards a quantum information network with squeezed light and entanglement,” 2003.

[17] T. C. Briles, D. C. Yost, A. Cingöz, J. Ye, and T. R. Schibli, “Simple piezoelectric-actuated mirror with 180 khz servo bandwidth,” *Optics express*, vol. 18, no. 10, pp. 9739–9746, 2010.

[18] “Siemens website: Natural frequency and resonance.” (), [Online]. Available: `https://community.sw.siemens.com/s/article/Natural-Frequency-and-Resonance`.

[19] “Piezodrive website: Pdu150 three channel ultra-low noise 150v piezo driver.” (), [Online]. Available: `https://www.piezodrive.com/modules/pdu150/`.

[20] S. Jutamulia, *Interferometers for measuring coherence length and high-speed switching of laser light*, US Patent 5,647,032, Jul. 1997.